

pubs.acs.org/acscatalysis Research Article

Selective Electrochemical CO₂ Reduction during Pulsed Potential Stems from Dynamic Interface

Kevin W. Kimura, Rileigh Casebolt, Jessica Cimada DaSilva, Elyse Kauffman, Jiyoon Kim, Tyler A. Dunbar, Christopher J. Pollock, Jin Suntivich, and Tobias Hanrath*



Cite This: ACS Catal. 2020, 10, 8632–8639



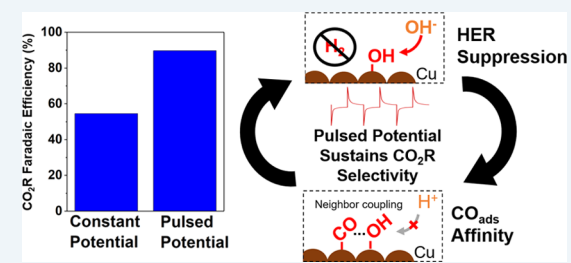
ACCESS

III Metrics & More

Article Recommendations

s Supporting Information

ABSTRACT: Pulsing the potential during the electrochemical CO₂ reduction (CO₂R) reaction using copper has been shown to influence product selectivity (i.e., to suppress the undesired hydrogen evolution reaction (HER)) and to improve electrocatalyst stability compared to the constant applied potential. However, the underlying mechanism and contribution of interfacial/surface phenomena behind the pulsed potential application remain largely unknown. We investigated the state of the copper surface during the pulsed potential electrochemical CO₂R using *in situ* X-ray adsorption near-edge spectroscopy (XANES). We probed the surface valence of the metallic electrode and found that the Cu electrode remains



metallic over a broad pulsed potential range and only oxidizes to form Cu(OH)₂ in the bulk when the pulsed potential reaches the highly oxidative limit (greater than 0.6 V vs reversible hydrogen electrode (RHE)). Our results suggest that the pulsed anodic potential influences the interfacial species on the electrode surface, i.e., the dynamic competition between protons and hydroxide adsorbates instead of bulk copper oxidation. We attribute the suppressed HER to the electroadsorption of hydroxides, which outcompetes protons for surface sites. As shown in a recent *in situ* infrared study [Iijima, G. et al.; ACS Catalysis 2019, 9, 6305], adsorbed hydroxides promote CO adsorption, a crucial CO₂ reduction intermediate, by preventing CO from becoming inert through a near-neighbor effect. We corroborate this interpretation by demonstrating that the pulsed potential application can suppress the HER during the CO reduction just as the CO₂R. Our results suggest that the pulsed potential mechanism favors CO₂R over the HER due to two effects: (1) proton desorption/displacement during the anodic potential and (2) the accumulation of OH_{ads} creating a higher pH—surface environment, promoting CO adsorption. We can describe this pulsed potential dynamic interfacial mechanism in a competing quaternary Langmuir isotherm model. The insights from this investigation have wide-ranging implications for applying pulsed potential profiles to improve other electrochemical reactions.

KEYWORDS: electrochemical CO₂ reduction, copper, pulsed potential, electrocatalysis, electrochemistry, interface

■ INTRODUCTION

The electrochemical CO₂ reduction (CO₂R) on copper electrodes in an aqueous electrolyte involves multiple competing reactions. The CO₂R itself is known to undergo multiple H⁺/e⁻ transfer processes to produce a variety of hydrocarbons (CO, CH₄, C₂H₄, etc.), while the hydrogen evolution reaction (HER) competes to produce H₂. Electrocatalytic reactions are governed by the interplay of mass transport to/from the electrode, surface adsorption/ desorption, and reaction kinetics, all of which dictate product selectivity. Therefore, significant research efforts to control product selectivity have focused on developing new electrocatalyst compositions/structures, ⁴ testing new electrolytes, ^{5,6} and improving reactor designs. ^{7–9} In a departure from the mainstream of these studies, the application of a pulsed potential is a less studied variable, which was recently shown to increase the degrees of experimental freedom to tailor product selectivity. 10 We have recently shown that millisecond pulses (a square-wave potential profile composed of an anodic and

cathodic potential) afford control over the product selectivity and suppress the undesired HER. 10,11 Moreover, pulsed potentials dynamically regenerate the surface and thereby have important implications for long-term operability by avoiding poisoning effects encountered in constant potential systems. In this work, we seek to move beyond the empirical relationship between pulse profile and product selectivity by tracking the copper electrode surface using *in situ* X-ray absorption spectroscopy (XAS). Elucidating the mechanism behind the pulsed electrosynthesis phenomenon will help advance our understanding of electrochemical interfaces, with

Received: June 15, 2020 Revised: June 19, 2020 Published: June 24, 2020





relevant technological implications in CO_2R and other electrosynthesis processes.

We consider two hypotheses on how the pulsed potential can affect the product selectivity. The first hypothesis considers the possibility that dynamic oxidation of the electrode surface changes the surface properties of the electrode. ¹² Specifically, we consider the possibility that copper oxides form during the anodic pulse and then the re-reduced copper during the next cathodic potential step may possess different catalytic properties, which would explain the change in observed selectivity. ¹³

The alternate hypothesis focused on the temporal concentration profile of intermediates bound to the electrode surface. 10 In this interpretation, the pulsed oxidative potential may preferentially adsorb favorable intermediate/ionic species to the surface, which would result in an improvement in $\rm CO_2R$ selectivity. In a preceding study, mass transport was found not to be a significant driving force behind the pulsing potential mechanism. 10 Below, we briefly discuss the underlying considerations and state of knowledge relevant to the two alternate hypotheses examined in this study.

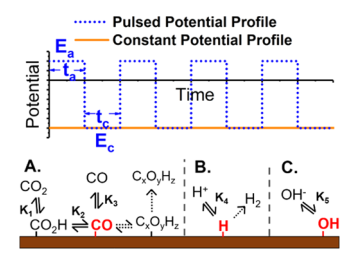
The nature of the copper electrode is known to significantly impact its electrocatalytic properties. For example, oxide-derived copper (OD-Cu) behaves differently from pristine copper. The preparation of various OD-Cu electrodes includes being air-annealed copper oxide films, electrochemically oxidized copper, and plasma-activated Cu⁺. Copper oxides have been shown to favor CO_2R at surprisingly low overpotentials, while $Cu(OH)_2$ -derived Cu has been shown to greatly favor C_{2+} products at higher overpotentials (-1 V vs reversible hydrogen electrode [RHE]).

Several groups have shown that the active sites on copper oxide materials are metallic copper that was reduced from the oxide phase. To understand how the OD-Cu differs from the conventional copper, Iijima et al. used *in situ* attenuated total reflection surface-enhanced infrared absorption spectroscopy (ATR-SEIRAS) and found that surface-adsorbed hydroxides (OHads) in OD-Cu promote CO adsorption at active Cu sites. Furthermore, they found that on pristine Cu, CO adsorbed/transferred from Cu atop to Cu bridge sites are inert and consequently deactivated the Cu surface. In contrast, the coupling between adsorbed OH on OD-Cu with bridge-site adsorbed CO prevented deactivation. We hypothesize that the introduction of a periodic anodic potential adsorbs OHads, which promotes CO adsorption on Cu active sites (COatop) and prevents inert CO adsorption on Cu bridge sites (CObridge), similar to what occurs in the OD-Cu.

Since electrochemical processes are interfacial phenomena, consideration of the absorbed species on the surface is critical. Ultimately, all product selectivity is dictated by the ability of the electrocatalyst to absorb intermediate species at various rates (K_i) during a reducing potential. As depicted in Scheme 1, we hypothesize that the pulsed potential dynamically changes the adsorption equilibrium (K_i) of the surface species $(CO, H^+, and OH^-)$ due to the periodically changing surface charge. Naturally, if the electro-absorbed surface species are different, the product selectivity distribution will be dramatically impacted. *In situ* spectroscopic techniques provide a powerful method to measure this phenomenon. 21,22

Here, we combine pulsed electrochemical experiments, in situ XAS, and a quaternary competitive Langmuir isotherm model to demonstrate that the pulsed potential mechanism is based on the dynamic interplay between four critical

Scheme 1. Constant Potential Profile (Orange) and Pulsed Potential Profile (Blue) Are Dictated by Adsorption Constants for the (A) CO₂ Reduction Reaction and Its Intermediates, (B) Proton Adsorption and Reduction, and (C) Hydroxide Adsorption^a



^aRed species indicate important adsorbed species of interest.

intermediate adsorbed species: $H_{ads}\text{, }OH_{ads}\text{, }CO_{atop,ads}\text{, }and$ $CO_{bridge,ads}\text{.}$

■ RESULTS AND DISCUSSION

Key differences in the product selectivity (i.e., Faradaic efficiency) for static and pulsed electrochemical CO_2 and CO reduction on polycrystalline Cu electrodes are summarized in Figure 1. The selectivity toward CO_2R is notably favored for

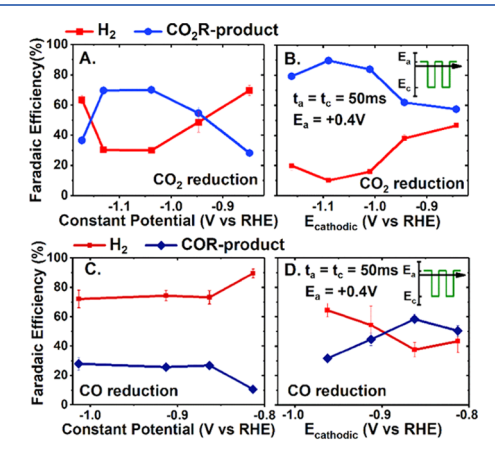


Figure 1. (A) FE of major CO_2 reduction products averaged over 1 h at the constant potential on polycrystalline Cu foil. (B) FE of major CO_2 reduction products averaged over 4 h using a pulsed potential profile. (C) Constant potential CO reduction on Cu. (D) Pulsed potential CO reduction on Cu.

the pulsed potential case (Figure 1B) compared to the constant potential (Figure 1A) $\mathrm{CO_2R}$. In Figure 1, we hold the pulsed reduction anodic potential (E_a), at +0.4 V vs RHE while varying the cathodic potential (E_c). The anodic and cathodic pulse times (t_a and t_c) were both kept at 50 ms. We limited the anodic potential to +0.4 V to avoid oxidation of the copper electrode (*vide infra*). We note that a more positive anodic potential of +0.6 V has previously been shown to further suppress HER Faradaic efficiency (FE) to <5%. ¹¹

The suppression of HER and increased favorability toward C-products are not limited to CO_2 . In Figure 1C,D, we compare the Faradaic efficiency for electrochemical CO reduction on a copper electrode between the constant vs pulsed potential. In the case of a pulsed potential, we observe a noticeable suppression in the HER selectivity. The improved CO selectivity implies that the pulsing mechanism is not specific to the first CO_2R intermediate species ($CO_2 + e^- \rightarrow CO_2R$)

 CO_2^-), which are not encountered in the CO reduction reaction pathway. This is significant because adsorbed CO_2^- species are considered to contribute the most to the reaction activation barrier (overpotential).^{2,23,24} We can interpret that CO reduction is also favored over HER with the application of a pulsed potential. Furthermore, Figure S1E-H shows that the pulsed potential suppresses the HER current density while increasing the CO_2R and COR current densities, respectively.

To understand the role of the anodic $(E_{\rm upper})$ and cathodic $(E_{\rm lower})$ pulse potential, we systematically varied the applied bias and examined the effect on Faradaic efficiency. For the experiments in Figure 1, $E_{\rm upper}$ was kept constant while $E_{\rm lower}$ was varied, resulting in HER suppression observed throughout the range of cathodic potentials. Next, we kept $E_{\rm lower}$ constant at -1.05 V while varying $E_{\rm upper}$, as shown in Figure 2 (green

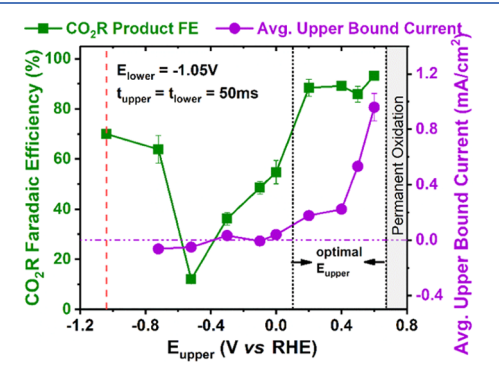


Figure 2. (Left axis) The FE (green) for the combined CO_2 reduction reaction products is shown for a range of $E_{\rm upper}$, while $E_{\rm lower}$ is kept at $-1.05~{\rm V}$ and the pulse interval was kept at 50 ms. (Right axis) Average upper-bound currents (purple) for the same range of varying $E_{\rm upper}$.

trace). The sum of the FEs for the major CO_2 products is shown, and the remaining FE is mainly attributed to HER. For comparison, the red dotted line represents the constant potential case. The equivalent partial current density is shown in Figure S2. The selectivity toward CO_2 reduction is poor when $E_{\rm upper}$ is between -0.6 and 0 V; however, above +0.2 V, selectivity toward CO_2 reduction improves when compared to the constant potential case. This trend suggests the presence of a potential threshold that must be crossed to effectively suppress HER. The average upper-bound current for the same range of $E_{\rm upper}$, as shown in Figure 2 (purple trace), indicates that poor selectivity to CO_2R correlates with the average upper-bound current close to 0 mA/cm² ($E_{\rm upper}$ in the range of 0 to -0.3 V). Details of the pulse current profile are provided in Figure S3B. This suggests that the upper-bound

potential dictates the degree of positive charge on the electrode surface, which in turn determines the degree of disruption of the interfacial adsorbates. A positive current would suggest that the electrode is positively charged during the upper-bound potential, while the lack of positive current suggests that the surface is not positively charged enough to disrupt the interfacial adsorbates. The trends in Figure 2 lead us to conclude that the electrode surface must reach a minimum positive charge to effectively suppress HER and promote $\mathrm{CO}_2\mathrm{R}$. It is important to note that the selectivity toward $\mathrm{CO}_2\mathrm{R}$ breaks down when E_{upper} is greater than +0.6 V as permanent surface oxidation of the copper electrode is observed, deactivating the electrode over time.

Having established the role of the anodic (upper bound) potential during pulsing, we moved on to investigate the valence state of the copper electrode when HER is suppressed $(+0.2 \text{ V} \le E_{\text{upper}} \le +0.6 \text{ V})$. We sought to understand whether the anodic pulse (E_{upper}) is actively oxidizing the Cu surface, adsorbing anions, or remaining in the reduced state. Details of the in situ XANES measurements to probe the copper valence at the surface of the electrode are provided in the Materials and Methods section. The inset in Figure 3A describes the in situ XANES experimental setup in which the electrode was composed of a 5 nm Cu thin film deposited on a silicon wafer with an Au/Ti adhesion layer. The CO2 saturated electrolyte layer was kept within 100 μ m to minimize the interaction between the X-ray and the electrolyte while allowing the product bubbles to be released. Raw Cu K-edge XANES spectra are provided in the Supporting Information (Figures S4-S6). To facilitate quantitative comparison of the spectra, each measurement was fit to a baseline-sigmoidal curve, and to two pseudo-Voigt curves (corresponding to the first two features of the Cu K-edge, Figure S4D) using a reserve Monte-Carlo optimization fit enabled by BlueprintXAS.²⁵ The methodology for determining fits is detailed in the Supporting Information.

Our *in situ* XANES analysis revealed that the Cu electrode is oxidized to $Cu(OH)_2$ (Figure S4). Using a best-fit ratio of Cu^0 to $Cu(OH)_2$ reference standard, the percentage of $Cu(OH)_2$ in the 5 nm Cu film is calculated with respect to applied constant potential (Figure 3A). The threshold of detectable change in valence occurred at a potential above constant +0.2 V vs RHE. This oxidative threshold is denoted as a red dotted line on the plot. Next, we pulsed the potential applied to the electrode and monitored the percentage of $Cu(OH)_2$ formed. In Figure 3B, the traces (i)—(vi) denote relevant pulse profiles in which t_a and t_c were kept at 50 ms, but E_a and E_c were varied. The corresponding E_a and E_c potentials are denoted in the above two plots. Despite E_a in the pulse profiles (iii)—(vi)

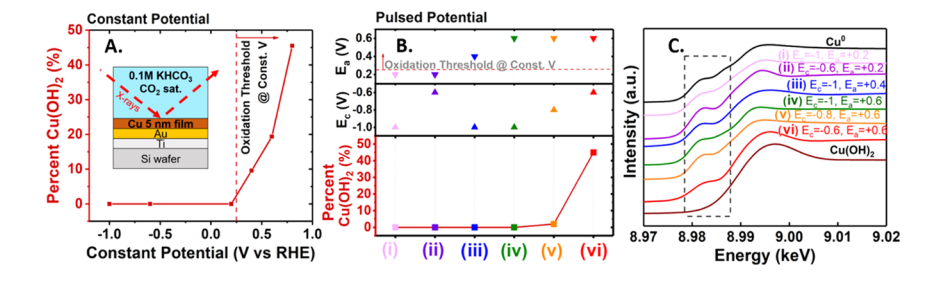


Figure 3. (A) Percentage of *in situ* surface $Cu(OH)_2$ over the range of potentials applied. Inset shows the *in situ* experimental setup. (B) Summary of the various anodic $V(E_a)$ and cathodic $V(E_c)$ of the pulsed profiles (color numbers) with the corresponding percentage oxidation $Cu(OH)_2/Cu^0$. (C) XANES scans of *in situ* pulsed potential CO_2R reaction on a Cu electrode.

being above the +0.2 V threshold determined in the constant potential case (Figure 3A), we do not see any noticeable accumulation of $Cu(OH)_2$ until the E_c is less negative than -0.8 V (i.e., above this value). This suggests that potential pulsing allows copper to momentarily pass the threshold that corresponds to the copper oxidation in the constant potential limit but without causing bulk copper oxidation. However, when the cathodic potential is not sufficiently reductive, such as at $E_c = -0.6$ V, the surface continually oxidizes and $Cu(OH)_2$ passivates into the bulk film. The *in situ* XANES spectra for the pulsed cases (i-vi) are shown in Figure 3C with the color matched to the corresponding pulse profile. When comparing Cu^0 to $Cu(OH)_2$, the most noticeable difference is that the peak at ~8.983 keV in the XANES spectra (dotted black box in Figure 3C) decreases with increasing Cu valence.

The pulsing profiles in which improved $\mathrm{CO}_2\mathrm{R}$ selectivity is observed (Figure 1B) remain in the window of operation, where $E_a < +0.6$ V and $E_c < -0.6$ V. At these pulsed profile regimes, there is no observable $\mathrm{Cu}(\mathrm{OH})_2$, which suggests that only the surface layer is changing, for example, by actively adsorbing and desorbing ions such as hydroxides. This greatly impacts the average surface coverage composition, as the oxidative potential during the pulsed potential application can bring negative ions (hydroxides) to the surface compared to the constant potential application, where the surface favors positive ions. We therefore conclude that pulsing causes the electrode to passivate with hydroxide ions to different degrees depending on the pulse profile without changing the bulk oxidation state of Cu^0 .

Surface hydroxides adsorbed on the electrode surface can react by displacing surface protons, thereby suppressing HER, while increasing the local pH, 26,27 which is known to improve $\mathrm{CO}_2\mathrm{R}$ electrocatalysis. The surface adsorbed hydroxides in $\mathrm{Cu}(\mathrm{OH})_2$ electrodes have been shown to promote $\mathrm{CO}_2\mathrm{R}$ by minimizing the formation of $\mathrm{CO}_{\mathrm{bridge}}$, an inert species, due to a near neighboring coupling effect. We, therefore, postulate that the surface hydroxides formed during the anodic potential contribute to the suppression of $\mathrm{CO}_{\mathrm{bridge}}$ formation during the pulsing. The anodic potential in the pulsed potential profile plays a key role in displacing adsorbed protons while creating a momentarily higher pH double-layer environment to prevent $\mathrm{CO}_{\mathrm{bridge}}$ formation.

The relationship between the anodic pulse and the transient high pH surface environment is further supported by an experiment in which a pulsed potential is switched to a constant potential and then switched back to a pulsed potential (Figure 4). A pulsed potential was first applied to a Cu electrode under CO₂R conditions until a steady-state FE was achieved. Then, the pulsed potential was switched to a constant potential (E = -1.05 V) for 1.5 h, followed by the initial pulsed potential profile being reintroduced. It is clear from Figure 4 that the pulsed potential maintains a suppressed H₂ FE, but when a constant potential is applied (at 75 min), the selectivity gradually favors HER. Note that during the first hour of constant potential, the FE of products matches the selectivity observed for 1 h of constant potential CO₂R;²⁹ however, the H2 FE dominates after the first hour of constant potential CO₂R. Finally, the constant potential was switched back to the starting pulsed potential profile (at 165 min). Upon reintroducing the pulsed potential, the FE of CO₂R products becomes once again favored, and HER selectivity is suppressed. This experiment shows that the pulsing effect is reversible and a transient effect; therefore, we conclude that

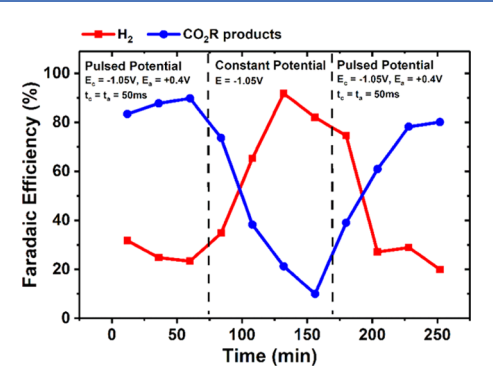


Figure 4. FE of major CO₂ reduction products (blue) and H₂ (red) over time, starting with a pulsed potential ($E_c = -1.05 \text{ V}$, $E_a = +0.4 \text{ V}$, $t_c = t_a = 50 \text{ ms}$), then switching to a constant potential (E = -1.05 V) for 1.5 h and finally switching back to the starting pulsed potential.

the pulsing mechanism lies within the electrode interface. We acknowledge that the electrode surface structure may be reordering; 27,30 however, a reordering of the surface structure back to the initial pristine Cu state during the constant potential phase at t=75 min is unlikely. This experiment displays the stable nature of applying a pulsed potential, as observed by a consistent product selectivity sustained over time, which cannot be explained by surface reordering.

We modeled the surface adsorption on the copper surface under the pulsed potential condition to test the interpretation of experiments and further refine the mechanistic interpretation. By simulating the surface concentration of the four adsorbates of interest, H_{ads} , OH_{ads} , $CO_{atop,ads}$, and $CO_{bridge,ads}$ during the constant vs pulsed potential cases, we visualize the steady-state concentration of adsorbed species on the surface.

The adsorption model builds upon a previously reported diffusion layer transport model. ^{10,31} For further details, we point to Gupta et al. ³¹

The results of the transport model give an electrode subsurface concentration of relevant species over time with the application of a constant or pulsed potential. The surface coverage is evaluated using the subsurface concentration of species calculated from the above transport model and a four-component (H_{ads} , OH_{ads} , $CO_{atop,ads}$, and $CO_{bridge,ads}$) competitive Langmuir isotherm (see the Supporting Information for a complete discussion of model calculations).

$$\theta_{i} = \frac{K_{\text{eq}}^{i} \Gamma_{i}}{1 + K_{\text{eq}}^{\text{CO}_{a}} \Gamma_{\text{CO}_{a}} + K_{\text{eq}}^{\text{CO}_{b}} \Gamma_{\text{CO}_{b}} + K_{\text{eq}}^{\text{H}_{2}} \Gamma_{\text{H}_{2}} + K_{\text{eq}}^{\text{OH}} \Gamma_{\text{OH}}}$$
(1)

 θ_i represents the fractional surface coverage of adsorbate i (H_{ads} , OH_{ads} , $CO_{atop,ads}$ or $CO_{bridge,ads}$), Γ_i is the surface coverage of adsorbate i, and K_{eq}^i is the equilibrium constant for adsorbate i and is defined as $k_{adsorption,i}$ over $k_{desorption,i}$. A Langmuir isotherm as described in eq 1 was assumed as it is the simplest model that broadly captures the complex nature of this four-component system. This adsorption model does not account for other possible species adsorbed onto the surface of the electrode such as K^+ , HCO_3^- , CO_3^{2-} , and other carbon species. A slow transfer reaction of $CO_{atop,ads}$ to $CO_{bridge,ads}$ is also assumed following a first-order reaction rate if minimal OH_{ads} is present, based on the findings of Iijima et al. 20 We approximated this rate constant to be constant $k=7.3e^{-4}$ s⁻¹. The details of the Langmuir isotherm model and the transfer rate are discussed in the Supporting Information. The

adsorption constants used are shown in Table 1, based on the polarity of H⁺/OH⁻ and *in situ* ATR-SEIRAS trends on Cu

Table 1. Assumed k_{ads} for the Constant and Pulsed Cases in the Competitive Langmuir Isotherm^a

$k_{ m ads}$, $E_{ m c}$		$k_{ m ads},~E_{ m a}$
$k_{ m ads,CO-atop}$	>	$k_{ m ads,CO-atop}$
$k_{ m ads,CO-bridge}$	>	$k_{ m ads,CO-bridge}$
$k_{ m ads,OH}$	«	$k_{ m ads,OH}$
$k_{ m ads,H}$	>>	$k_{ m ads,H}$

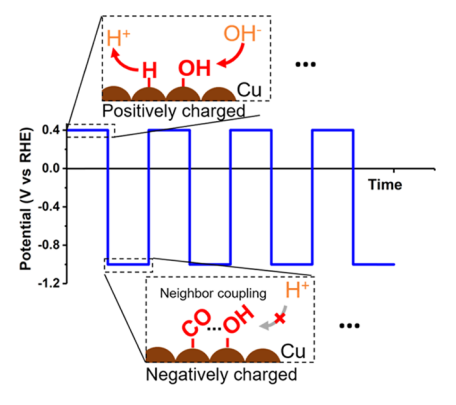
">" corresponds to a factor of 3, denoting a small change in the surface affinity. ">> or «" corresponds to a factor of 10, denoting a large change in the surface affinity due to a change in polarity.

tracked over time. 21,32 The pulse time intervals in the model were kept to $t_a = t_c = 50$ ms to model the same time profiles used in the experiments shown in Figure 1. Based on these assumptions, the normalized surface coverage for the four species is shown in Figure 5. Figure 5A suggests that the pulsed potential favors the accumulation of OH_{ads} compared to the constant potential case where hydroxide formation is suppressed, consistent with the result observed by Iijima et al.²⁰ Additionally, H_{ads} is suppressed with the introduction of a pulsed potential due to the competing nature of the adsorbed species and OH_{ads} blocking the surface, which could react by displacing the adsorbed proton, as shown in Figure 5B. Finally, the normalized surface coverage of CO_{atop} and CO_{bridge} does not change with pulsing at early time scales; however, over longer time scales, the higher concentration of hydroxides in the pulsed potential case help to maintain CO_{atop} accumulation compared to the constant potential case, where CO_{bridge} accumulation overtakes CO_{atop}.

Whereas the exact adsorption constants, $k_{\rm ads}$, are difficult to determine, we can gain qualitative insight by comparing their relative magnitudes and plotting the resulting relative surface coverages. Figure 5 demonstrates how the fractional surface coverage will dynamically differ between the constant potential and pulsed potential cases. A sensitivity analysis of the relative adsorption rates further upheld the general trends observed in Figure 5 (see the Supporting Information for details).

In summary, the dynamic change in surface coverage during the pulsed potential application occurs if the anodic potential passes an oxidative potential above +0.2 V. The electrode surface becomes positively charged above +0.2 V, which repels H⁺ and favors OH⁻ adsorption, as visualized in Scheme 2. This process of rapid changes in the interfacial adsorbate composition will inevitably disrupt site-blocking cations in the outer Helmholtz plane,³³ which could lead to possible electrocatalysis enhancement not accounted for in the adsorption model.²⁶ As an added benefit, the electrode

Scheme 2. Schematic Describing the Dynamic Surface Coverage during the Anodic and Cathodic Potentials^a



^aThe surface protons will be repelled and displaced by hydroxides during the anodic pulse. During the cathodic potential, the remaining surface hydroxides will induce near neighbor coupling with CO, favoring CO₂R.

maintains stability by self-cleaning the surface from impurities, which would otherwise reduce onto the surface and poison the electrocatalyst. Above +0.6 V vs RHE, however, the anodic potential causes accumulation of $\text{Cu}(\text{OH})_2$, which eventually inactivates the electrode. The cathodic potential maintains the reduced state of the Cu and creates a high pH surface environment, where residual OH_{ads} remain on the surface, inducing the near-neighbor coupling interaction with CO_{ads} . This promotes CO adsorption in general and suppresses the undesired CO_{atop} to $\text{CO}_{\text{bridge}}$ transformation. Eventually, the increased accumulation of CO_{ads} and OH_{ads} on the surface, as shown by Figure 5, blocks H adsorption sites to suppress HER.

The vital role of surface hydroxides agrees and builds upon the work by Le Duff et al. in which surface oxygen species were hypothesized to increase selectivity toward CO2R during pulsed voltammetry and pulsed potential reduction on a singlecrystal Cu electrode in a phosphate buffer.³⁴ In this work, we tie in the importance of OH_{ads} relation to CO_{ads} as well as the displacement of H_{ads} with OH_{ads} as an explanation for the observed CO₂R enhancement during the potential pulsing. The temporary nature of the pulsing effect further emphasizes that this increase in selectivity is likely a result of a dynamic phenomenon within the electrode interface and not due to an inherent change in the bulk electrode composition, as is the case with OD-Cu. Finally, the effect of "cleaning off" heavy metal contaminants and other organic species is not considered in our model or mechanism, although it may play a role in enhancing CO₂R selectivity.

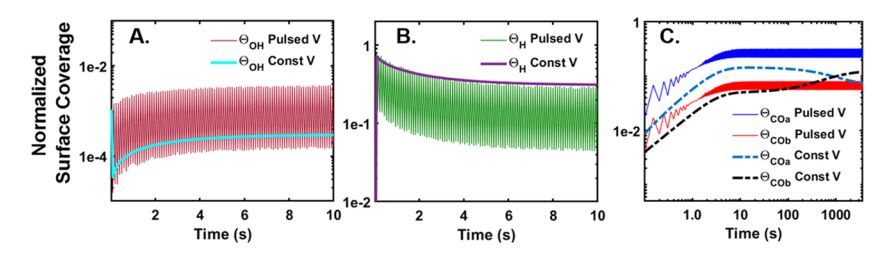


Figure 5. Relative surface coverage assuming a competitive quaternary Langmuir isotherm comparing pulsed vs constant potential of (A) adsorbed OH over 10 s, (B) adsorbed H over 10 s, and (C) adsorbed CO_{atop} and CO_{bridge} over 1 h, where the pulse profile assumes ($t_a = t_c = 50 \text{ ms}$).

ACS Catalysis pubs.acs.org/acscatalysis Research Article

CONCLUSIONS

This work explores a possible mechanism to explain how pulsed potential electrochemical CO₂R leads to a shift in the adsorbate coverage, which favors CO2R. We found that the application of pulsed potential also suppresses the HER during the CO reduction. This suggests that the pulsed potential mechanism involves CO, a known crucial intermediate for CO₂R. In situ XANES was used to probe the copper electrode during the pulsing experiment. We observed no accumulation of oxides within the regime of CO₂R-selective pulsed potential profiles. Based on the observed anodic current but lack of the copper oxidation, we hypothesize that hydroxides are adsorbed on the surface during the upper (anodic) potential swing of the potential pulsing, suggesting that surface OH_{ads} plays a crucial role during the pulse potential mechanism. The pulsed anodic potential acts to disrupt site-blocking cations in the outer Helmholtz plane and displace Hads with OHads, which maintains a higher local pH near the electrode surface. The higher pH surface environment results in residual OHads interacting with nearest neighbor CO_{ads} and preventing CO_{bridge} formation. Our proposed dynamic interface mechanism can be described using a semiempirical competing quaternary Langmuir isotherm model. These findings also align well with results published on OD-Cu, where CO2R occurs at lower overpotentials with higher selectivity and improved stability.20

The application of pulsed potentials in electrochemical conversion reactions has implications beyond ${\rm CO_2}$ reduction as favorability could be tuned for other competing electrochemical reactions. We imagine a dynamically changing surface charge could be modified to favor specific organic electrosynthesis products as well as modulate other complex electrochemical processes.

MATERIALS AND METHODS

Preparation of Copper Electrodes for Electrochemical CO₂ and CO Reduction. Copper foil (99.99+%, Alfa Aesar) was used as the working electrode. Following the same procedure as previously reported, 10 the electrodes were connected to a titanium wire (0.75 mm diameter, Goodfellow) using Leitsilber 200 silver paint (Ted Pella) and then later covered in an inert two-part Omegabond 101 epoxy (Omega), with only the desired working electrode geometric area exposed (~0.2 cm²). The inert epoxy was thoroughly mixed for at least 5 min and cured in a dry box for at least 48 h. A successful epoxy cure was confirmed when the epoxy had a matte sheen and no tactile stickiness. Right before each electrochemical measurement, the electrode was electropolished using a new 85% phosphoric acid solution by applying a 1 A current for a duration of 1 s, followed by a thorough rinsing of the surface using deionized Milli-Q water. All deionized water used throughout the study was Milli-Q

Electrochemistry. A conventional three-electrode setup was utilized in a custom glass H-cell. The glass cell was thoroughly cleaned before each experiment in a nitric acid boil followed by a deionized water boil bath. The catholyte and anolyte chambers in the H-cell were separated by a Nafion N-117 membrane (Alfa Aesar) and rubber gasket. All nonglass parts in the glass cell were thoroughly rinsed and sonicated in deionized water. Both the catholyte (15 mL) and anolyte (7 mL) chambers held solutions of 0.1 M KHCO₃ (Sigma-

Aldrich) electrolyte. The 0.1 M KHCO $_3$ electrolyte was chelated using Chelex100 (Sigma-Aldrich) for at least 12 h before use to remove any heavy metal impurities. The catholyte electrolyte was saturated with research 200 grade CO $_2$ (Airgas) for 10 min before each CO $_2$ reduction experiment. Likewise, the catholyte was saturated with CO (Airgas) for 10 min before each CO reduction experiment. All experiments for CO were performed with all components of the experimental setup in a well-ventilated hood with at least two CO detectors present. A platinum mesh counter electrode (approximate area \sim 12 cm 2) was submerged in the anolyte chamber, and the Ag/AgCl reference electrode (Pine Instruments) with the prepared copper working electrode was placed in the catholyte chamber.

A Bio-Logic SP-150 potentiostat (Bio-Logic Science Instruments) was used with the accompanying EC-Lab software to perform the electrochemical measurements. The potentials for the chronoamperometry were measured and calculated using previously reported methods with iR correction. The pulsed potential experiments were performed by looping between two potentials (E_c and E_a) at the desired time intervals (t_c and t_a). The electrochemical reduction was performed for typically 1 h in the constant potential case and 4 h for the pulsed potential case. During these time scales, the product selectivity achieved was fairly consistent.

Product Analysis of Electrochemical CO₂ and CO **Reduction.** CO₂ gas was bubbled into the H-cell catholyte chamber during the electrochemical measurements at a rate of 1.4 mL/min using an El-Flow Select CO₂ mass-flow controller (Bronkhorst). CO gas was bubbled using a rotameter at a rate of 1 mL/min (Omega). The outlet gas directly fed into a gas chromatograph (GC, SRI Instruments, Multiple Gas Analyzer #5), which detected the gas compositions using a thermal conductivity detector (to quantify H2) and flame ionization detector (to quantify CH₄, CO, CO₂, C₂H₄). The carrier gas for the GC was UHP Grade 5.0 argon (Airgas), and the hydrogen source came from a hydrogen generator (H2-100 SRI Instruments). The first GC gas sample was taken 10 min after the start of each electrochemical measurement to ensure that the system had reached a steady state. Each GC sample took 18 min to separate through the columns and 8 min to rest flush the columns. Calibration gases were diluted and used to calibrate the GC measurements at relevant concentrations of gas products.

Liquid products were measured via ¹H nuclear magnetic resonance spectroscopy (NMR; Bruker AV500) by following reported methods²⁹ to detect all major liquid products: ethanol, formic acid, acetaldehyde, acetate, and *n*-propanol. A known concentration of dimethyl sulfoxide (Sigma-Aldrich) was used as a reference value in the NMR sample. Deuterium oxide was also used to suppress the water signal in the NMR sample. Four hundred microliters of the liquid electrolyte was used in each NMR sample. Known concentrations of the hydrocarbons were used to create calibration curves to validate the measurement method.

Preparation of Copper Electrodes for *In Situ* XANES Measurements. The electrodes were prepared in a clean-room environment. The electrodes were prepared using a CVC SC4500 E-gun evaporation system (CVC), where 20 nm of Ti was deposited on a Si wafer, followed by 10 nm of Au and by 5 nm of Cu. Thickness was measured by the quartz crystal microbalance. The thin-film electrodes were cut into 5 mm × 10 mm rectangles using a Disco dicing saw (Disco). Copper

(II) oxide powder (98+%, Krackeler Scientific) copper (I) oxide powder (97+%, Krackeler Scientific) and copper (II) hydroxide (95+%, Krackeler Scientific) were used for reference spectra.

In Situ XANES Measurements. *In situ* copper K-edge XAS data were collected at the C1 beamline of the Cornell High Energy Synchrotron Source with ring conditions of 5.3 GeV and ~110 mA. A custom Teflon cell was used to perform in situ XAS. The setup, as shown in Scheme S1, consisted of electrolyte reservoirs, which ensured electrolyte coverage of the electrode, and a thin channel for the electrode. There was a 100 µm gap between the electrode surface and the Kapton film, which covered the in situ cell and held in the electrolyte. The electrolyte was bubbled and saturated with CO₂ before the experiment. Incident X-rays were energy selected using a Si(220) double crystal monochromator, and energy calibration was achieved by setting the first inflection point of a copper foil scan to 8979 eV. The beam was focused on the sample in a 1 mm × 5 mm spot, and spectra were collected in fluorescence mode using a four-element Vortex detector positioned at 90° relative to the incident beam. Each XANES scan covered the range of 8850-9200 eV in 5 eV steps except in the range of 8960-9010 eV in finer 0.5 eV steps and took about 20 min to complete. The upper- and lower-bound energy regions were used to set the normalization of the spectra. In between each scan, the cell was checked on to make sure no bubble blockages occurred or electrolyte was depleted.

ASSOCIATED CONTENT

Supporting Information

The Supporting Information is available free of charge at https://pubs.acs.org/doi/10.1021/acscatal.0c02630.

Fitting the *in situ* XANES data; expanded details of main figures; and details/sensitivity analysis of the adsorption model (PDF)

AUTHOR INFORMATION

Corresponding Author

Tobias Hanrath — Robert F. Smith School of Chemical and Biomolecular Engineering, Cornell University, Ithaca, New York 14853, United States; orcid.org/0000-0001-5782-4666; Email: th358@cornell.edu

Authors

Kevin W. Kimura — Robert F. Smith School of Chemical and Biomolecular Engineering, Cornell University, Ithaca, New York 14853, United States; oorcid.org/0000-0003-4238-9731

Rileigh Casebolt — Robert F. Smith School of Chemical and Biomolecular Engineering, Cornell University, Ithaca, New York 14853, United States

Jessica Cimada DaSilva — Robert F. Smith School of Chemical and Biomolecular Engineering, Cornell University, Ithaca, New York 14853, United States; orcid.org/0000-0002-8108-5557

Elyse Kauffman — Robert F. Smith School of Chemical and Biomolecular Engineering, Cornell University, Ithaca, New York 14853, United States

Jiyoon Kim — Material Science & Engineering, Cornell University, Ithaca, New York 14853, United States

Tyler A. Dunbar — Robert F. Smith School of Chemical and Biomolecular Engineering, Cornell University, Ithaca, New York 14853, United States; oorcid.org/0000-0003-2971-5766 Christopher J. Pollock — Cornell High Energy Synchrotron Source (CHESS), Wilson Laboratory, Cornell University, Ithaca, New York 14853, United States; ⊙ orcid.org/0000-0001-5736-513X

Jin Suntivich — Material Science & Engineering, Cornell University, Ithaca, New York 14853, United States; orcid.org/0000-0002-3427-4363

Complete contact information is available at: https://pubs.acs.org/10.1021/acscatal.0c02630

Author Contributions

The manuscript was written through the contributions of all authors. All authors have given approval to the final version of the manuscript.

Notes

The authors declare no competing financial interest.

ACKNOWLEDGMENTS

This work was supported in part by the National Science Foundation (NSF; CBET1805400). K.W.K. was supported by the NSF Graduate Research Fellowship and Cornell University Department of Chemical Engineering McMullen Fellowship. R.C. was supported by the Robert F. Smith School of Chemical and Biomolecular Engineering. J.C.d.S. was supported by Capes, Brazil (13159/13-5). This work made use of the Cornell Center for Materials Research Shared Facilities, which are supported through the NSF MRSEC program (DMR-1120296). This work is based upon research conducted at the Cornell High Energy Synchrotron Source (CHESS), which is supported by the National Science Foundation under award DMR-1332208. The authors would like to thank Dr. C. Pollock, Dr. K. Finkelstein, Dr. P. Ko, and Dr. R. Huang for their assistance with the XAS experiments. The authors would also like to thank David Wise for building the custom glass

ABBREVIATIONS

XAS, X-ray adsorption spectroscopy; XANES, X-ray adsorption near edge spectroscopy; HER, hydrogen evolution reaction; CO₂R, carbon dioxide reduction; FE, Faradaic efficiency; RHE, reversible hydrogen electrode; ATR-SEIRAS, attenuated total reflectance surface-enhanced infrared spectroscopy; OD-Cu, oxide-derived copper; KHCO₃, potassium bicarbonate; GC, gas chromatograph; NMR, nuclear magnetic resonance spectroscopy

■ REFERENCES

- (1) Hori, Y. Electrochemical CO₂ Reduction on Metal Electrodes. In *Modern Aspects of Electrochemistry*; Springer: New York, 2008; pp 89–189.
- (2) Peterson, A. A.; Abild-Pedersen, F.; Studt, F.; Rossmeisl, J.; Nørskov, J. K. How Copper Catalyzes the Electroreduction of Carbon Dioxide into Hydrocarbon Fuels. *Energy Environ. Sci.* **2010**, *3*, 1311.
- (3) Costentin, C.; Robert, M.; Savéant, J.-M. Catalysis of the Electrochemical Reduction of Carbon Dioxide. *Chem. Soc. Rev.* **2013**, 42, 2423–2436.
- (4) Nitopi, S.; Bertheussen, E.; Scott, S. B.; Liu, X.; Engstfeld, A. K.; Horch, S.; Seger, B.; Stephens, I. E. L.; Chan, K.; Hahn, C.; Nørskov, J. K.; Jaramillo, T. F.; Chorkendorff, I. Progress and Perspectives of Electrochemical CO₂ Reduction on Copper in Aqueous Electrolyte. *Chem. Rev.* **2019**, *119*, 7610–7672.
- (5) Zhao, G.; Jiang, T.; Han, B.; Li, Z.; Zhang, J.; Liu, Z.; He, J.; Wu, W. Electrochemical Reduction of Supercritical Carbon Dioxide in

- Ionic Liquid 1-n-Butyl-3-Methylimidazolium Hexafluorophosphate. *J. Supercrit. Fluids* **2004**, 32, 287–291.
- (6) Rosen, B. A.; Salehi-Khojin, A.; Thorson, M. R.; Zhu, W.; Whipple, D. T.; Kenis, P. J. A.; Masel, R. I. Ionic Liquid-Mediated Selective Conversion of CO₂ to CO at Low Overpotentials. *Science* **2011**, 334, 643–644.
- (7) Inaba, M.; Jensen, A. W.; Sievers, G. W.; Escudero-Escribano, M.; Zana, A.; Arenz, M. Benchmarking High Surface Area Electrocatalysts in a Gas Diffusion Electrode: Measurement of Oxygen Reduction Activities under Realistic Conditions. *Energy Environ. Sci.* **2018**, *11*, 988–994.
- (8) Higgins, D.; Hahn, C.; Xiang, C.; Jaramillo, T. F.; Weber, A. Z. Gas-Diffusion Electrodes for Carbon Dioxide Reduction: A New Paradigm. ACS Energy Lett. 2019, 4, 317–324.
- (9) Weekes, D. M.; Salvatore, D. A.; Reyes, A.; Huang, A.; Berlinguette, C. P. Electrolytic CO₂ Reduction in a Flow Cell. *Acc. Chem. Res.* **2018**, *51*, 910–918.
- (10) Kimura, K. W.; Fritz, K. E.; Kim, J.; Suntivich, J.; Abruña, H. D.; Hanrath, T. Controlled Selectivity of CO₂ Reduction on Copper by Pulsing the Electrochemical Potential. *ChemSusChem* **2018**, *11*, 1781–1786.
- (11) Kimura, K. W.; Suntivich, J.; Hanrath, T. In Controlled Selectivity of CO₂ Reduction on Metal Electrodes By Pulsing the Electrochemical Potential, ECS Meeting, 2018; MA2018-01.
- (12) Kumar, B.; Brian, J. P.; Atla, V.; Kumari, S.; Bertram, K. A.; White, R. T.; Spurgeon, J. M. Controlling the Product Syngas H₂:CO Ratio through Pulsed-Bias Electrochemical Reduction of CO₂ on Copper. ACS Catal. **2016**, *6*, 4739–4745.
- (13) Li, C. W.; Kanan, M. W. CO₂ Reduction at Low Overpotential on Cu Electrodes Resulting from the Reduction of Thick Cu₂O Films. *J. Am. Chem. Soc.* **2012**, *134*, 7231–7234.
- (14) Ren, D.; Deng, Y.; Handoko, A. D.; Chen, C. S.; Malkhandi, S.; Yeo, B. S. Selective Electrochemical Reduction of Carbon Dioxide to Ethylene and Ethanol on Copper(I) Oxide Catalysts. *ACS Catal.* **2015**, *5*, 2814–2821.
- (15) Roberts, F. S.; Kuhl, K. P.; Nilsson, A. High Selectivity for Ethylene from Carbon Dioxide Reduction over Copper Nanocube Electrocatalysts. *Angew. Chem., Int. Ed.* **2015**, *54*, 5179–5182.
- (16) Mistry, H.; Varela, A. S.; Bonifacio, C. S.; Zegkinoglou, I.; Sinev, I.; Choi, Y.-W.; Kisslinger, K.; Stach, E. A.; Yang, J. C.; Strasser, P.; Cuenya, B. R. Highly Selective Plasma-Activated Copper Catalysts for Carbon Dioxide Reduction to Ethylene. *Nat. Commun.* **2016**, *7*, No. 12123.
- (17) Mandal, L.; Yang, K. R.; Motapothula, M. R.; Ren, D.; Lobaccaro, P.; Patra, A.; Sherburne, M.; Batista, V. S.; Yeo, B. S.; Ager, J. W.; Martin, J.; Venkatesan, T. Investigating the Role of Copper Oxide in Electrochemical CO₂ Reduction in Real Time. ACS Appl. Mater. Interfaces 2018, 10, 8574–8584.
- (18) Klingan, K.; Kottakkat, T.; Jovanov, Z. P.; Jiang, S.; Pasquini, C.; Scholten, F.; Kubella, P.; Bergmann, A.; Cuenya, B. R.; Roth, C. Reactivity Determinants in Electrodeposited Cu Foams for Electrochemical CO₂ Reduction. *ChemSusChem* **2018**, *11*, 3449–3459.
- (19) Eilert, A.; Roberts, F. S.; Friebel, D.; Nilsson, A. Formation of Copper Catalysts for CO₂ Reduction with High Ethylene/Methane Product Ratio Investigated with In Situ X-Ray Absorption Spectroscopy. *J. Phys. Chem. Lett.* **2016**, *7*, 1466–1470.
- (20) Iijima, G.; Inomata, T.; Yamaguchi, H.; Ito, M.; Masuda, H. Role of a Hydroxide Layer on Cu Electrodes in Electrochemical CO₂ Reduction. *ACS Catal.* **2019**, *9*, 6305–6319.
- (21) Dunwell, M.; Lu, Q.; Heyes, J. M.; Rosen, J.; Chen, J. G.; Yan, Y.; Jiao, F.; Xu, B. The Central Role of Bicarbonate in the Electrochemical Reduction of Carbon Dioxide on Gold. *J. Am. Chem. Soc.* **2017**, *139*, 3774–3783.
- (22) Heyes, J.; Dunwell, M.; Xu, B. CO₂ Reduction on Cu at Low Overpotentials with Surface-Enhanced in Situ Spectroscopy. *J. Phys. Chem. C* **2016**, *120*, 17334–17341.
- (23) Amatore, C.; Saveant, J. M. Mechanism and Kinetic Characteristics of the Electrochemical Reduction of Carbon Dioxide

- in Media of Low Proton Availability. J. Am. Chem. Soc. 1981, 103, 5021-5023.
- (24) Costentin, C.; Robert, M.; Savéant, J.-M. Catalysis of the Electrochemical Reduction of Carbon Dioxide. *Chem. Soc. Rev.* **2013**, 42, 2423–2436.
- (25) Delgado-Jaime, M. U.; Mewis, C. P.; Kennepohl, P. Blueprint XAS: A Matlab-Based Toolbox for the Fitting and Analysis of XAS Spectra. J. Synchrotron Radiat. 2010, 17, 132–137.
- (26) Strain, J. M.; Gulati, S.; Pishgar, S.; Spurgeon, J. M. Pulsed Electrochemical Carbon Monoxide Reduction on Oxide-Derived Copper Catalyst. *ChemSusChem* **2020**, *13*, 1–7.
- (27) Arán-Ais, R. M.; Scholten, F.; Kunze, S.; Rizo, R.; Cuenya, B. R. The Role of in Situ Generated Morphological Motifs and Cu(i) Species in C₂₊ Product Selectivity during CO₂ Pulsed Electroreduction. *Nat. Energy* **2020**, *5*, 317–325.
- (28) Hori, Y.; Takahashi, R.; Yoshinami, Y.; Murata, A. Electrochemical Reduction of CO at a Copper Electrode. *J. Phys. Chem. B* **1997**, *101*, 7075–7081.
- (29) Kuhl, K. P.; Cave, E. R.; Abram, D. N.; Jaramillo, T. F. New Insights into the Electrochemical Reduction of Carbon Dioxide on Metallic Copper Surfaces. *Energy Environ. Sci.* **2012**, *5*, 7050.
- (30) Gunathunge, C. M.; Li, X.; Li, J.; Hicks, R. P.; Ovalle, V. J.; Waegele, M. M. Spectroscopic Observation of Reversible Surface Reconstruction of Copper Electrodes under CO₂ Reduction. *J. Phys. Chem. C* 2017, 121, 12337–12344.
- (31) Gupta, N.; Gattrell, M.; MacDougall, B. Calculation for the Cathode Surface Concentrations in the Electrochemical Reduction of CO₂ in KHCO₃ Solutions. *J. Appl. Electrochem.* **2006**, *36*, 161–172.
- (32) Wuttig, A.; Ryu, J.; Surendranath, Y. Electrolyte Competition Controls Surface Binding of CO Intermediates to CO₂ Reduction Catalysts. 2019, https://doi.org/10.26434/chemrxiv.7929038.v1.
- (33) Murata, A.; Hori, Y. Product Selectivity Affected by Cationic Species in Electrochemical Reduction of CO₂ and CO at a Cu Electrode. *Bull. Chem. Soc. Jpn.* **1991**, *64*, 123–127.
- (34) Le Duff, C. S.; Lawrence, M. J.; Rodriguez, P. Role of the Adsorbed Oxygen Species in the Selective Electrochemical Reduction of CO₂ to Alcohols and Carbonyls on Copper Electrodes. *Angew. Chem., Int. Ed.* **2017**, *56*, 12919–12924.